Proceedings of the Reactor Physics Asia 2023 (RPHA2023) Conference
Gyeongju, Korea, October 24-26, 2023

Generating Multigroup Cross-Sections via Monte Carlo Method for Fast Reactor Analysis: A Concise Review

Hui Guo[1,*], Yiwei Wu[1], Qufei Song[1], Kuaiyuan Feng[1], Hanyang Gu[1]
[1] *School of Nuclear Science and Engineering, Shanghai Jiao Tong University, Shanghai, China*
[*] *Corresponding author: hui.guo@sjtu.edu.cn*

1. Introduction

Efficient and accurate neutronics modeling is paramount to advancing novel nuclear systems. The complex geometry, diverse neutron spectrum, extensive burnup, and space kinetics pose difficult challenges to neutronics analysis tools. The Monte Carlo (MC) method excels in leveraging high-fidelity geometry, explicit anisotropic representation, and continuous energy (CE) cross-section libraries, thereby demonstrating exceptional accuracy. Nevertheless, the MC method often demands substantial computational resources, notably for tasks such as multiphysics coupling, fuel management optimization, depletion simulations, and transient analysis.

In contrast, deterministic methods offer distinctly faster simulations by employing spatial discretization approximations, simplified angle representations, and energy structure reductions. These deterministic codes find extensive application in core analysis, particularly for multiphysics and depletion assessments. However, their efficacy depends significantly on the utilization of effective multigroup cross-sections (MGXS).

Modeling the fast neutron spectrum, which predominantly resides within the keV and MeV range, necessitates a comprehensive treatment of anisotropic scattering, inelastic scattering, (n,2n) reactions, and the intricate phenomenon of unresolved resonance self-shielding[1]. The fast spectrum exhibit a neutron mean-free path that is approximately an order of magnitude longer, thereby amplifying the sensitivity to neutron leakage and even minor variations in core geometry[2]. The generation of MGXS using MC code is widely investigated and implemented[3,4]. This method integrates the resonance self-shielding and spatial homogenization under a CE representation and an almost arbitrary level of spatial detail. Therefore, there is a growing interest in generation of MGXS using MC method for fast reactor analysis.

This paper presents a concise review of the generation of MGXS utilizing MC methods, along with their integration with both diffusion and transport core solvers. In Section 2.1, we outline the fundamental approach for generating MGXS using MC codes. In Section 2.2, we provide a summary of the key findings in the existing literature. Sections 2.3 and 2.4 delve into specific topics: Section 2.3 examines the superhomogénéisation equivalent techniques (SPH), while Section 2.4 explores the flux-moment homogenization techniques (MHT). Finally, in Section 3, we present our conclusions.

2. Methods and Results

In this section, the general method of MGXS generation using the MC method is presented, then the existing results are summarized, and finally, SPH and MHT techniques are discussed.

2.1 General method

The generation of MGXS was widely developed in MC method codes, for instance, SERPENT[3], MCNP6[5], McCARD[6], RMC[7], OpenMC[4], MCS[8,9] and MCX[10]. The flux-volume homogenization method, widely used in most MC codes, is presented in this section.

2.1.1. General cross-sections

n the OpenMC code, the macroscopic cross-section of nuclide 'i' within spatial region 'k' and energy range [E_{g-1}, E_g], is defined as the quotient of the group-wise reaction rates $\langle \Sigma_{x,i}, \psi \rangle_{k,g}$ and fluxes $\langle \psi \rangle_{k,g}$ tallied by the track-length estimators.

$$\Sigma_{x,i,k,g} = \frac{\langle \Sigma_{x,i}, \phi \rangle_{k,g}}{\langle \phi \rangle_{k,g}} \quad (1)$$

$$\langle \Sigma_{x,i}, \phi \rangle_{k,g} = \int_{\boldsymbol{r} \in V_k} d\boldsymbol{r} \int_{4\pi} d\boldsymbol{\Omega} \int_{E_g}^{E_{g-1}} dE \Sigma_x(\boldsymbol{r}, E) \psi(\boldsymbol{r}, E, \boldsymbol{\Omega}) \quad (2)$$

$$\langle \phi \rangle_{k,g} = \int_{\boldsymbol{r} \in V_k} d\boldsymbol{r} \int_{4\pi} d\boldsymbol{\Omega} \int_{E_g}^{E_{g-1}} dE \psi(\boldsymbol{r}, E, \boldsymbol{\Omega}) \quad (3)$$

Under this definition, $\Sigma_{t,i,k,g}$, $\Sigma_{s,i,k,g}$, $\nu\Sigma_{f,i,k,g}$ and $\kappa\Sigma_{f,i,k,g}$ are computed. In this work, the microscopic cross-section by nuclide is generated then by

$$\sigma_{x,i,k,g} = \frac{\Sigma_{x,i,k,g}}{N_{i,k}} \quad (4)$$

where $N_{i,k}$ is the concentration of nuclide *i* in region *k.* Microscopic cross-sections are employed to facilitate perturbation and depletion calculations in subsequent analyses. However, it's important to note that utilizing microscopic cross-sections will lead to an augmented computational load in terms of tallying, memory utilization, and data storage requirements.

2.1.2. Consistent scattering matrix

In the work, the consistent scattering matrix is used, which is computed as the product of the scattering cross-sections $\Sigma_{s,i,k,g}$ tallied by the track-length estimator and the group-to-group probabilities $P_{s\ell,i,k,g' \to g}$. The consistent formulation ensures that reaction rate balance

is exactly preserved as other cross-sections are computed using a track-length estimator.

The scatter matrix at Legendre order ℓ is defined as:

$$\Sigma_{s\ell,i,kg'\to g} = \Sigma_{s,i,k,g} \times P_{s\ell,i,k,g'\to g} \quad (5)$$

where the scattering probability matrix is computed from analog tallies:

$$P_{s\ell,i,k,g'\to g} = \frac{\langle \Sigma_{s\ell,i}, \phi \rangle_{k,g}}{\langle \Sigma_{s0,i}, \phi \rangle_{k,g}} \quad (6)$$

where $P_\ell(\Omega \cdot \Omega')$ is the Legendre polynomials at order ℓ.

In the following, the cross-sections with scattering matrix at order ℓ is represented by the abbreviation P_ℓ.

2.1.3. Scattering multiplicity

The scattering matrix is multiplied by the multiplicity matrix $\upsilon_{i,k,g'\to g}$ to incorporate the effect of neutron multiplication from (n,*x*n) reactions.

$$\Sigma_{s\ell,i,k,g'\to g} = \upsilon_{i,k,g'\to g} \times \Sigma_{s,i,k,g} \times P_{s\ell,i,k,g'\to g} \quad (7)$$

The multiplicity matrix is computed by:

$$\upsilon_{i,k,g'\to g} = \frac{\langle \upsilon_i \Sigma_{s,i}, \phi \rangle_{k,g}}{\langle \Sigma_{s,i}, \phi \rangle_{k,g}} \quad (8)$$

2.1.4. Transport correction

The transport-corrected total cross-sections (Σ_{tr}) and transport-corrected scattering matrix (Σ_{str}) are required for mitigating the isotropic scattering approximation. The TCP_0 is used as the abbreviation for using Σ_{tr} and Σ_{str}. The P_0 transport correction is applied, and the TCP_0 cross-sections are computed as follows:

$$\Sigma_{tr,i,k,g} = \frac{\langle \Sigma_{t,i}, \phi \rangle_{k,g} - \langle \Sigma_{s1,i}, \phi \rangle_{k,g}}{\langle \phi \rangle_{k,g}} \quad (9)$$

$$\Sigma_{str,g'\to g} = \frac{\langle \Sigma_{s,0,g'\to g} \phi \rangle - \delta_{gg'} \sum_{g''} \langle \Sigma_{s1,g''\to g} \phi \rangle}{\langle \phi \rangle} \quad (10)$$

where $\delta_{gg'}$ is the Kronecker delta function.

The diffusion coefficients used in this work is defined as:

$$D_{i,k,g} = \frac{1}{3\Sigma_{tr,i,k,g}} \quad (11)$$

For the rigorous and computationally efficient computation of diffusion coefficients and transport cross-sections in light water reactors, we introduce a novel approach termed the Cumulative Migration Method (CMM)[11–15]. This method effectively mitigates the sources of inaccuracy inherent in the widely employed "out-scatter" transport correction technique.

2.2 Review of results

The results of coupling the MGXS generated through the MC method and the multigroup deterministic/MC solver are summarized in Table I. These two-step sequences mainly include Serpent-DYN3D[16], Serpent-VARIANT[17], MCS-RAST[8], MCS-MCS(MG)[8], Serpent-Griffin[18], OpenMC-TRIVAC[19], OpenMC-OpenMC(MG)[20,21]. These results are obtained from different size fast reactors cooled by sodium or lead and fueled with UOX, MOX, metallic, carbide fuels, and nitride fuel.

2.2.1 Diffusion solvers

Utilizing the diffusion solver, the bias between the two-step approach and the reference MC method fluctuates within the range of -163 to 263 pcm. In a majority of outcomes, MGXS were derived from 2D/3D super-cell configurations, encompassing elaborate layouts of fuel and structural assemblies. The Monte Carlo methodology affords remarkable flexibility in selecting models for MGXS generation. The MET-1000 core analysis, employing both the Serpent-Griffin and OpenMC schemes, adopts a comprehensive 3D whole-core model.

The integration with diffusion solvers has demonstrated strong predictive capabilities for core reactivity estimation. Nevertheless, a common observation in much of the literature is the significant overestimation of control rod worth attributed to this approach. The locally heterogeneous modeling of absorbers has enhanced accuracy in control rod worth[22,23], while this strategy might not be feasible for the majority of core solvers. Alternatively, another avenue to mitigate this bias is the employment of SPH techniques, as elaborated upon in Section 2.3.

In the Serpent/Griffin scheme, a whole core SPH technique is used and reduces the overestimation to 0 pcm which is an interesting research direction in generating MGXS from a 3D full-core model. This whole core SPH equivalent technique is also proved with the CEFR start-up test benchmark and with micro-reactors[24]. The MC can generate the whole core reaction rate and MGXS at the same time, which enables to correct MGXS for conserving exactly the reaction rate at a specified state. This is an attractive feature in multiphysics modelling while the robustness of the SPH factors in perturbation should be further verified.

2.2.2 Transport solvers

When employing a transport solver or a multigroup MC solver, a notable tendency for reactivity overestimation becomes evident. For instance, within the Serpent/VARIANT scheme, a 2D MET-1000 core displays a substantial overestimation of 643 pcm. Similarly, utilizing the multigroup MC approach yields a 1087 pcm overestimation in a 3D MET-1000 core with OpenMC, and a 1085 pcm overestimation with MCS. Adopting the OpenMC/Trivac setup with an SP5 solver exhibits an 880 pcm overestimation.

It's important to highlight that both MC and SPN multigroup transport solvers manifest this pattern of overestimating core reactivity when MGXS are generated using the MC method based on the general approach illustrated in Section 2.1. This consistent

overestimation highlights the need for careful consideration and potentially more refined methodologies in MGXS generation.

The application of flux-moment homogenization brings about a significant reduction in the overestimation of core reactivity, mitigating it from 1087 pcm to 374 pcm for the MET-1000 scenario within the OpenMC-OpenMC(MG) scheme. Further elaboration on this topic will be provided in Section 2.4.

Table I: Reactivity in reference (units: pcm)

XS code	Core solver	Core	Difference(3)	Reference
Serpent	DYN3D	OECD/NEA 3600-MOX	-128	[25]
		PHENIX (350 MW_{th}, MOX)	-162	[26]
		FFTF (400 MW_{th}, MOX)	-152	[27]
		SPX (3000MW_{th}, MOX)	-63	[28]
Serpent	PARCS	OECD/NEA 3600-MOX	-84	[25]
Serpent	VARIANT	OECD/NEA MET-1000 (2D)	+643(4)	[17]
MCS	RAST-K	OECD/NEA MET-1000	+41	[8]
		OECD/NEA 3600-MOX	+105	[8]
MCS	MCS-MG(1)	OECD/NEA MET-1000	+1085	[8]
		OECD/NEA 3600-MOX	+444	[8]
MCS	RAST-F	OECD/NEA MET-1000	-34	[9]
		OECD/NEA CAR-3600	+126	[9]
		CEFR (65 MW_{th}, UOX)	+58	[29]
		ANTS-100e (100 MW_e, UN, LBE)	+77	[30]
Serpent	Griffin	VTR (300 MW_{th}, UPuZr)	+263	[18]
			0(5)	[18]
OpenMC	OpenMC-MG(2)	OECD/NEA MET-1000	+1087	[31]
			+374(6)	[31]
		SVBR (100 MW_e, UOX, LBE)	+255(7)	[32]
OpenMC	OpenMC-MG	CEFR (65 MW_{th}, UOX)	+1729(8)	[20]
	TRIVAC		-105(9)	
OpenMC	Trivac	OECD/NEA MET-1000	+242(10)	[19]
			+880(11)	[19]

Remarks: (1) Multigroup MC calculation with TCP_0 MGXS; (2) Multigroup MC calculation with P_5 MGXS; (3) Results are compared to the MC CE method if not specified; (4) Nodal transport solver with P5 scattering matrix; (5) With SPH in whole core regions; (6) With flux-moment homogenization techniques; (7) Reflector is simplified as LBE; (8) Compared to experiments results; (9) With SPH in whole core regions and compared to experiments results; (10) Diffuse solver with TCP_0 MGXS; (11) Transport solver with P_5 MGXS.

2.3 SPH equivalent techniques

The SPH equivalent techniques[33,34] are widely used to preserve the reaction rates of a reference heterogeneous model and a homogenous model. In [35,8,9,19,24], the SPH techniques are used by coupling the MC MGXS generation and the nodal diffusion solving to improve the accuracy of control rod modeling.

The sketch of the SPH generation process used in this work is shown in Fig. 1:

Step#1: Initial heterogeneous geometry models are used to generate reference heterogeneous flux and MGXS of the homogenized region using MC continuous-energy calculation.

Step#2: MGXS generated in Step#1 are used in MC multigroup calculation of the corresponding case in homogenized geometry and obtained homogenized flux.

Step#3: SPH factor for homogenized region r and energy group g is calculated as:

$$\mu_{r,g} = \frac{\overline{\varphi_{r,g}^{hete}}}{\varphi_{r,g}^{homo}} N_g \tag{12}$$

where $\overline{\varphi_{r,g}^{hete}}$ is total reference flux in the corresponding homogenized region, $\varphi_{r,g}^{homo}$ is homogenized flux in the homogenized region, N_g is the normalization factor calculated[36]:

$$N_g = \frac{\sum_r \overline{\varphi_{r,g}^{ref}}}{\sum_r \varphi_{r,g}^{homo}} \tag{13}$$

Step#4: Modify initial MGXS $\Sigma_{r,m,g}$ by multiplying SPH factors. For homogenized space m and energy group g, the corrected cross-section $\Sigma_{r,m,g}^{Mod}$ is calculated as:

$$\Sigma_{r,m,g}^{Mod} = \mu_{m,g}\Sigma_{r,m,g} \tag{14}$$

Step#5: Modified MGXS are applied in Step#2 and repeat Step#2 to Step#4 to obtain SPH factors of a new generation until SPH factors satisfy the convergence condition.

The SPH technique is characterized by a fixed-point iterative process that necessitates the generation of cross-sections and flux solely once within the heterogeneous model. This particular attribute holds significant importance as it effectively alleviates the computational load.

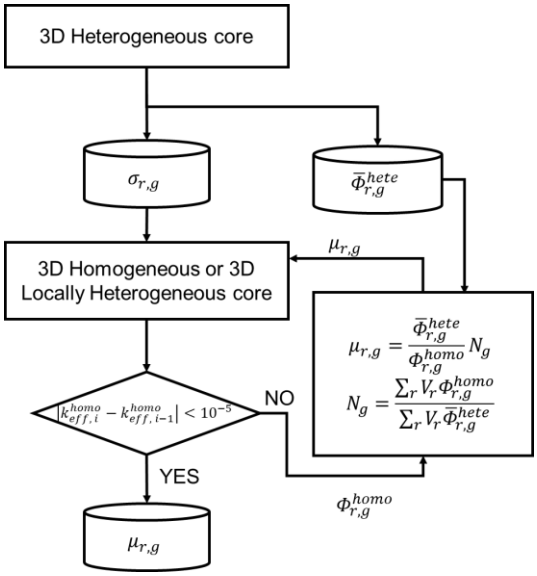

Fig. 1. Iteration scheme of SPH factor generation[19]

In the context of the MET-1000, a comparison of the S-curves for control rods is presented in Fig. 2, contrasting results obtained from OpenMC-Trivac with and without the employment of SPH techniques[19]. The overestimation associated with the TCP0/Diffusion approach escalates from 3.8% to 13.5% upon the insertion of control rods. Upon incorporating SPH correction, the relative errors exhibited by the TCP0+SPH/Diffusion approach range from -7.5% to 0.4%. Notably, the TCP0+SPH/Diffusion methodology displays exceptional performance when control rods are substantially inserted. However, it's important to acknowledge that this scheme is not as adaptable to cases involving slight control rod insertions, necessitating further investigation.

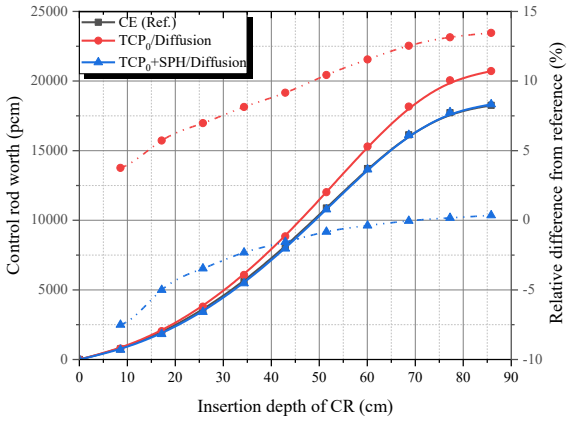

Fig. 2. S-curve of control rods[19]

Fig. 3 illustrates the substantial enhancement in the accuracy of power distribution prediction brought about by the utilization of SPH techniques. For the TCP0+SPH/Diffusion schemes, the maximum and minimum errors stand at 3.2% and -4.2%, respectively, across all control rod insertions.

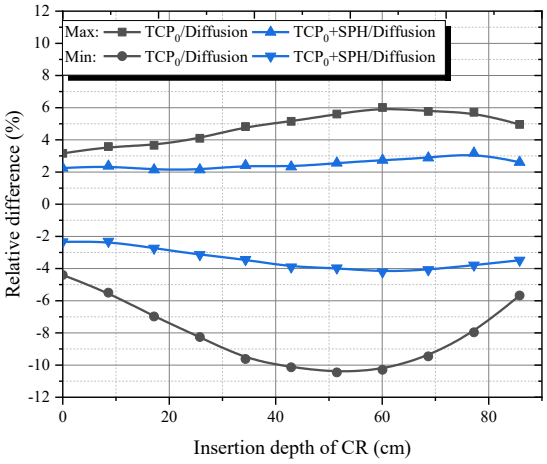

Fig. 3. Variation of relative maximal and minimal error with the insertion of control[19]

2.4 Flux-moment homogenization techniques

In most deterministic transport codes, MGXS are independent of the incident angle. In Reference [37] and Reference [38], the 'consistent-P' approximation[39] is generalized to 2D and 3D for fast reactor analysis and called the flux-moment homogenization technique (MHT). The MHT was implemented in OpenMC[31].

The concept of flux-moment homogenization relies on neutron conservation principles. The fundamental stationary Boltzmann neutron transport equation can be expressed as follows:

$$L(r,\Omega) + T(r,\Omega) = S(r,\Omega) + F(r,\Omega) \quad (15)$$

where the term 'L' signifies leakage, the term 'T' represents the total reaction rate, the term 'S' denotes the scattering source, and the term 'F' corresponds to the fission term. Developing the angular flux and transfer XS in spherical harmonics $Y_{\ell,m}$ in T and S gives:

$$T = \Sigma^G_{k,t}\psi_k(\Omega) = \sum_{\ell}\frac{2\ell+1}{4\pi}\sum_{m=-l}^{\ell}\Sigma^G_{k,t}\varphi^G_{k,\ell,m}Y_{\ell,m}(\Omega) \quad (16)$$

$$S = \sum_{G'}\sum_{\ell}\frac{2l+1}{4\pi}\sum_{m=-\ell}^{\ell}\Sigma^{G'\to G}_{k,s,\ell,m}\,\varphi^{G'}_{k,\ell,m}Y_{\ell,m}(\Omega) \quad (17)$$

However, if the angle dependence of the total cross-sections is considered, the exact equation is:

$$L(r,\Omega) + \tilde{T}(r,\Omega) = S(r,\Omega) + F(r,\Omega) \quad (18)$$

where the angle-dependency is also taken into account by a spherical harmonics expansion:

$$\tilde{T} = \Sigma^G_{k,t}(\Omega)\psi_k(\Omega) = \sum_{\ell}\frac{2\ell+1}{4\pi}\sum_{m=-\ell}^{\ell}\Sigma^G_{k,t,\ell,m}\varphi^G_{k,\ell,m}Y_{\ell,m}(\Omega) \quad (19)$$

To keep an isotropic total cross-section in simulation, the T term should be considered on the left side of the equation, leading to:

$$L + T = S + T - \tilde{T} + F \tag{20}$$

Notice that the flux terms in S, T and $\tilde{T}$ are the same and they can be combined:

$$\hat{S} = S + T - \tilde{T} = \sum_{G'}\sum_{\ell}\frac{2\ell+1}{4\pi}\sum_{m=-\ell}^{\ell}(\Sigma_{k,s,\ell,m}^{G'\to G} + \delta_{G,G'}(\Sigma_{k,t}^{G} - \Sigma_{k,t,\ell,m}^{G}))\varphi_{k,\ell,m}^{G}Y_{\ell,m}(\Omega) \tag{21}$$

Equivalent scattering matrices can be obtained:

$$\hat{\Sigma}_{k,s,\ell,m}^{G'\to G} = \Sigma_{k,s,\ell,m}^{G'\to G} + \delta_{GG'}(\Sigma_{k,t}^{G} - \Sigma_{k,t,\ell,m}^{G}) \tag{22}$$

In doing so, we have to deal with spherical harmonic moments for the scattering matrices. The dataset form is still complex and with poor generality. To fit the isotropic form of XS data, Vidal et al. proposed a collapsing method based on the least square method to collapse spherical harmonic moments into Legendre moments[38]:

$$\hat{\Sigma}_{k,s,\ell}^{G'\to G} = \Sigma_{k,s,\ell}^{G'\to G} + \delta_{GG'}(\Sigma_{k,t}^{G} - \Sigma_{k,t,\ell}^{G}) \tag{23}$$

where:

$$\Sigma_{k,t,\ell}^{G} = \frac{\sum_{-\ell}^{\ell}\varphi_{k,\ell,m}^{G}R_{k,t,\ell,m}^{G}}{\sum_{-\ell}^{\ell}\varphi_{k,\ell,m}^{G}{}^{2}} \tag{24}$$

where $R_{k,t,\ell,m}^{G}$ and $\varphi_{k,\ell,m}^{G}$ can be directly tallied in the MC code.

The reference [38] refers to numerical divergence when MGXS with MHT is used in the deterministic method. A fix-up is used to set the corrected high-order scattering matrices to no more than zero-order scattering matrices to avoid divergence:

$$if\ \left|\hat{\Sigma}_{k,s,\ell}^{G'\to G}\right| > \Sigma_{k,s,0}^{G'\to G},\ let\ \hat{\Sigma}_{k,s,\ell}^{G'\to G} = \Sigma_{k,s,0}^{G'\to G}\cdot\frac{\hat{\Sigma}_{k,s,\ell}^{G'\to G}}{\left|\hat{\Sigma}_{k,s,\ell}^{G'\to G}\right|} \tag{25}$$

The MHT changes the angle distribution of the scattering reaction to represent the anisotropy of the total cross-sections. The correction should be appropriate to all transport solvers.

The outcomes achieved through MHT homogenization for MET-1000 core with OpenMC/OpenMC(MG) scheme are depicted in Fig. 4. The overall disparity of MC-MGXS without correction amounts to approximately 1192 pcm when employing Legendre order 3. This difference can be attributed to the angle-dependent nature of cross-sections, resulting in a bias of around 772 pcm. MHT substantially mitigates much of this effect, accounting for 698 pcm. The residual 74 pcm come from an insufficient expansion order and the angle-dependence of cross-sections other than Σ_t. Increasing the scattering order from 3 to 7 leads to a reduction of approximately 120 pcm in reactivity bias, while spatial and energy homogenization introduces a bias of about 172 pcm. The remaining bias of 128 pcm remains unexplained for now; potential contributions include inaccuracies in anisotropic scattering representations.

The deviations in power distribution are illustrated in Fig. 5. The analysis of the power distribution reveals a tendency in the multi-group transport results to overestimate power in peripheral assemblies and underestimate it in central assemblies. Utilizing MGXS without MHT yields notable maximum radial biases of 4.02%/-4.10%, along with axial biases of 3.03%/-3.63%. The Root Mean Square Error (RMSE) for this configuration stands at 1.54%.

Incorporating MHT into the MC-MGXS approach substantially ameliorates these biases. Radial biases are reduced to 2.76%/-2.39%, while axial biases are mitigated to 0.79%/-2.25%. As a result, the RMSE is effectively lowered to 0.76%. This correction leads to a reduction in both the overestimation of peripheral assemblies and the underestimation of central assemblies, confirming the capability of MC-MGXS with MHT to effectively counteract the bias introduced by the angle dependence of Σ_t.

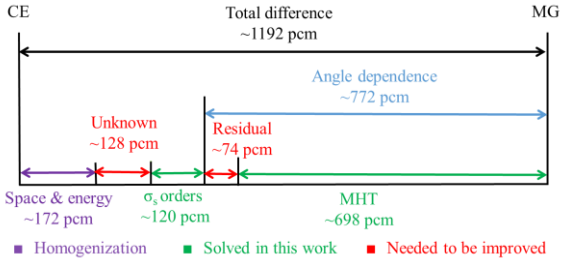

Fig. 4. Decomposition of the reactivity bias between CE and multigroup MC results[31]

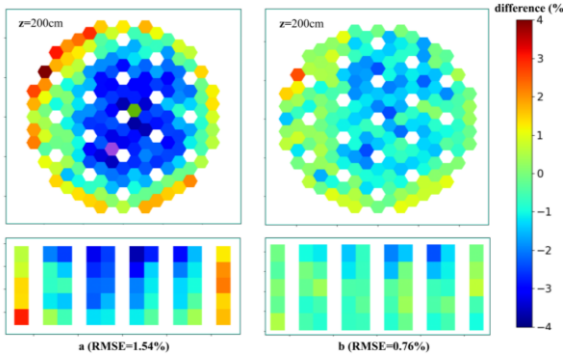

Fig. 5. Power distribution bias at all-rods-out (a: w/o MHT; b: w/i MHT)[31]

3. Conclusions

The utilization of the Monte Carlo (MC) method for generating multi-group cross sections (MGXS) offers the advantage of eliminating the resonance approximation and facilitating the treatment of intricate 2D/3D geometries. In the context of the advancing capabilities of high-performance computers, this method has become increasingly appealing. This article presents a comprehensive review of its application in the analysis of fast reactors, particularly through the integration of diffusion and transport solvers. The paper outlines the general methodology employed and subsequently provides a summary of results obtained across various types of fast reactors with the use of different computational codes. Moreover, the discussion extends to cover thesuperhomogénéisation equivalent techniques

(SPH) and the flux-moment homogenization techniques (MHT). Finally, in Section 3, we present our conclusions., both of which play significant roles in enhancing the accuracy of the presented approach.

The available results show that the coupling with diffusion solver exhibits good accuracy in the prediction of the effective multiplication factor whole overtimes the absorbers' effect. The SPH techniques improve its accuracy in predicting control rod worth. Remarkably, the synergistic application of SPH and a 3D whole-core MGXS generation model achieves the exact conservation of reaction rates under specified conditions.

When coupled with a transport solver, utilizing scalar flux volume homogenization techniques tends to result in an overestimation of the effective multiplication factor. However, this overestimation can be mitigated by employing the MHT technique, which effectively addresses the issue by accounting for the anisotropic effect of total cross-sections within the scattering matrix.

The statistical uncertainty of MGXS requires further quantification to ensure the reliability of the results. Additionally, it's imperative to assess the robustness of SPH factors under perturbations states. The validation of MHT techniques across a variety of reactor types is necessary. Furthermore, the application of MHT to transport-corrected cross-sections needs further studied.

It's worth noting that this brief review of MGXS generated using the MC method lacks a comprehensive survey of their performance in areas such as power distribution, feedback coefficients, perturbated states, and computational efficiency. These aspects should also be explored for a more comprehensive understanding of the method's capabilities and limitations.

ACKNOWLEDGMENT

This study is sponsored by National Natural Science Foundation of China (No. 12105170, 12135008) and Science and Technology on Reactor System Design Technology Laboratory.

REFERENCES

[1] Yang W S. Fast reactor physics and computational methods[J]. NUCLEAR ENGINEERING AND TECHNOLOGY, 2012: 22.

[2] Sofu T. A review of inherent safety characteristics of metal alloy sodium-cooled fast reactor fuel against postulated accidents[J]. Nuclear Engineering and Technology, 2015, 47(3): 227–239.

[3] Leppänen J, Pusa M, Fridman E. Overview of methodology for spatial homogenization in the Serpent 2 Monte Carlo code[J]. Annals of Nuclear Energy, 2016, 96: 126–136.

[4] Boyd W, Nelson A, Romano P K, Shaner S, Forget B, Smith K. Multigroup Cross-Section Generation with the OpenMC Monte Carlo Particle Transport Code[J]. Nuclear Technology, 2019, 205(7): 928–944.

[5] Goorley T, James M, Booth T, Brown F, Bull J, Cox L J, Durkee J, Elson J, Fensin M, Forster R A, Hendricks J, Hughes H G, Johns R, Kiedrowski B, Martz R, Mashnik S, McKinney G, Pelowitz D, Prael R, Sweezy J, Waters L, Wilcox T, Zukaitis T. Taylor & Francis, 2012. Initial MCNP6 Release Overview[J]. Nuclear Technology, 2012, 180(3): 298–315.

[6] Park H J, Shim H, Joo H, Kim C. Qualification test of few group constants generated from an MC method by the two-step neutronics analysis system McCARD/MASTER[J]. undefined, 2011.

[7] Wang K, Li Z, She D, Liang J, Xu Q, Qiu Y, Yu J, Sun J, Fan X, Yu G. RMC – A Monte Carlo code for reactor core analysis[J]. Annals of Nuclear Energy, 2015, 82: 121–129.

[8] Nguyen T D C, Lee H, Lee D. Use of Monte Carlo code MCS for multigroup cross section generation for fast reactor analysis[J]. Nuclear Engineering and Technology, 2021, 53(9): 2788–2802.

[9] Tran T Q, Cherezov A, Du X, Lee D. Verification of a two-step code system MCS/RAST-F to fast reactor core analysis[J]. Nuclear Engineering and Technology, 2021, 54(5): 1789–1803.

[10] Qin S, Li Y, He Q, Cao L, Wang Y, Wu Y, Wu H. Homogenized cross-section generation for pebble-bed type high-temperature gas-cooled reactor using NECP-MCX[J]. Nuclear Engineering and Technology, 2023, 55(9): 3450–3463.

[11] Liu Z, Smith K, Forget B. Progress of Cumulative Migration Method for computing diffusion coefficients with OpenMC[C]//, 2017.

[12] Liu Z, Giudicelli G, Smith K, Forget B. Conservation of migration area by transport cross sections using Cumulative Migration Method in deterministic heterogeneous reactor transport analysis[J]. Progress in Nuclear Energy, 2020, 127: 103447.

[13] Liu Z, Smith K, Forget B. Group-wise tally scheme of incremental migration area for cumulative migration method[J]. , 2018.

[14] Liu Z, Smith K, Forget B, Ortensi J. Cumulative migration method for computing rigorous diffusion coefficients and transport cross sections from Monte Carlo[J]. Annals of Nuclear Energy, 2018, 112: 507–516.

[15] Liu Z, Smith K, Forget B. Calculation of multi-group migration areas in deterministic transport simulations[J]. Annals of Nuclear Energy, 2020, 140: 107110.

[16] Nikitin E. Extension of the nodal code DYN3D to SFR applications[D]. , 2016.

[17] Lin C-S, Yang W S. An assessment of the applicability of multigroup cross sections generated with Monte Carlo method for fast reactor analysis[J]. Nuclear Engineering and Technology, 2020, 52(12): 2733–2742.

[18] Martin N, Stewart R, Bays S. A multiphysics model of the versatile test reactor based on the MOOSE

framework[J]. Annals of Nuclear Energy, 2022, 172: 109066.

[19] Guo H, Wu Y, Song Q, Cong T, Gu H. Development of OpenMC/Trivac two-step scheme for fast reactor core neutronics analysis[J]. Annals of Nuclear Energy, 2023, 190.

[20] Guo H, Feng K, Wu Y, Jin X, Huo X, Gu H. Preliminary verification of multi-group cross-sections generation and locally heterogeneous transport calculation using OpenMC with CEFR start-up tests benchmark[J]. Progress in Nuclear Energy, 2022, 154(104484).

[21] Guo H, Wu Y, Song Q, Shen Y, Gu H. Development of multi-group Monte-Carlo depletion calculation method and verification with metallic fast reactor[J]. Nuclear Science and Techniques, 2022, Under Review.

[22] Guo H, Garcia E, Faure B, Buiron L, Archier P, Sciora P, Rimpault G. Advanced method for neutronic simulation of control rods in sodium fast reactors: Numerical and experimental validation[J]. Annals of Nuclear Energy, 2019, 129: 90–100.

[23] Guo H, Archier P, Vidal J-F, Buiron L. Advanced method for depletion calculation of control rods in sodium fast reactors[J]. Annals of Nuclear Energy, 2019, 129: 160–168.

[24] Wu Y, Song Q, Xu H, Hu J, Gu H, Guo H. Generation of multi-group cross-sections for microreactor with whole-core superhomogenization equivalence technique[C]//ICONE. , 2023Kyoto, Japan: .

[25] Nikitin E, Fridman E, Mikityuk K. Solution of the OECD/NEA neutronic SFR benchmark with Serpent-DYN3D and Serpent-PARCS code systems[J]. Annals of Nuclear Energy, 2015, 75: 492–497.

[26] Nikitin E, Fridman E. Extension of the reactor dynamics code DYN3D to SFR applications – Part II: Validation against the Phenix EOL control rod withdrawal tests[J]. Annals of Nuclear Energy, 2018, 119: 411–418.

[27] Nikitin E, Fridman E. Modeling of the FFTF isothermal physics tests with the Serpent and DYN3D codes[J]. Annals of Nuclear Energy, 2019, 132: 679–685.

[28] Ponomarev A, Mikityuk K, Zhang L, Nikitin E, Fridman E, Álvarez-Velarde F, Romojaro Otero P, Jiménez-Carrascosa A, García-Herranz N, Lindley B, Baker U, Seubert A, Henry R. Superphénix Benchmark Part I: Results of Static Neutronics[J]. Journal of Nuclear Engineering and Radiation Science, 2022, 8(1): 011320.

[29] Tran T Q. Neutronic simulation of the CEFR experiments with the nodal diffusion code system RAST-F[J]. Nuclear Engineering and Technology, 2022: 15.

[30] Nguyen T D C, Tran T Q, Lee D. Coupled neutronics/thermal-hydraulic analysis of ANTS-100e using MCS/RAST-F two-step code system[J]. Nuclear Engineering and Technology, 2023.

[31] Wu Y, Song Q, Feng K, Vidal J-F, Gu H, Guo H. Multigroup cross-sections generated using Monte-Carlo method with flux-moment homogenization technique for fast reactor analysis[J]. Nuclear Engineering and Technology, 2023.

[32] Wu Y, Song Q, Wang R, Xiao Y, Gu H, Guo H. Development and verification of a Monte Carlo two-step method for lead-based fast reactor neutronics analysis[J]. Nuclear Engineering and Technology, 2023.

[33] Kavenoky A. The SPH homogenization method[J]. , 1980.

[34] Hébert A. CEA-N-2209, 1981. Développement de la méthode SPH: Homogénéisation de cellules dans un réseau non uniforme et calcul des parametres de réflecteur[D]. , 1981.

[35] Nikitin E, Fridman E, Mikityuk K. On the use of the SPH method in nodal diffusion analyses of SFR cores[J]. Annals of Nuclear Energy, 2015, 85: 544–551.

[36] Labouré V, Wang Y, Ortensi J, Schunert S, Gleicher F, DeHart M, Martineau R. Hybrid super homogenization and discontinuity factor method for continuous finite element diffusion[J]. Annals of Nuclear Energy, 2019, 128: 443–454.

[37] Vidal J-F, Archier P, Calloo A, Jacquet P, Tommasi J. An improved energy-collapsing method for core-reflector modelization in sfr core calculations using the paris platform[C]//PHYSOR 2012. , 2012Knoxville, Tennessee, USA: : 15.

[38] Vidal J-F, Archier P, Faure B, Jouault V, Palau J-M, Pascal V, Rimpault G, Auffret F, Graziano L, Masiello E, Santandrea S. APOLLO3® homogenization techniques for transport core calculations - application to the ASTRID CFV core[J]. Nuclear Engineering and Technology, 2017, 49: 1379–1387.

[39] Qiu R, Ma X, Xu Q, Liu J, Chen Y. American Society of Mechanical Engineers, 2017. Development and Verification of Multi-Group Cross Section Process Code TXMAT for Fast Reactor RBEC-M Analysis[C]//Volume 3: Nuclear Fuel and Material, Reactor Physics and Transport Theory; Innovative Nuclear Power Plant Design and New Technology Application. , 2017Shanghai, China: : V003T02A015.